Effect of random disorder and spin frustration on the reentrant spin-glass and ferromagnetic phases in the stage-2 $Cu_{0.93}Co_{0.07}Cl_2$ graphite intercalation compound near the multicritical point

Itsuko S. Suzuki* and Masatsugu Suzuki†

Department of Physics, State University of New York at Binghamton, Binghamton, New York 13902-6000, USA

(Received 13 August 2005; revised manuscript received 17 February 2006; published 29 March 2006)

The stage-2 $Cu_{0.93}Co_{0.07}Cl_2$ graphite intercalation compound magnetically behaves like a reentrant ferromagnet near the multicritical point ($c_{MCP} \approx 0.96$). It undergoes two magnetic phase transitions at T_{RSG} ($=6.64 \pm 0.05$ K) and T_c ($=8.62 \pm 0.05$ K). The static and dynamic nature of the ferromagnetic and reentrant spin-glass phase has been studied using dc and ac magnetic susceptibility. Characteristic memory phenomena of the dc susceptibility are observed at T_{RSG} and T_c. The nonlinear ac susceptibility χ'_3 has a positive local maximum at T_{RSG}, and a negative local minimum at T_c. The relaxation time τ between T_{RSG} and T_c shows a critical slowing down: τ with $x=13.1 \pm 0.4$ and $\tau_0^* = (2.5 \pm 0.5) \times 10^{-13}$ s. The influence of the random disorder on the critical behavior above T_c is clearly observed: $\alpha = -0.66$, $\beta = 0.63$, and $\gamma = 1.40$. The exponent of α is far from that of the three-dimensional Heisenberg model.

DOI: 10.1103/PhysRevB.73.094448 PACS number(s): 75.10.Nr, 75.50.Lk, 75.40.Gb, 75.30.Kz

I. INTRODUCTION

Magnetic phase transitions in reentrant ferromagnets are one of the most intriguing topics which have been extensively studied in recent years.[1–5] The competing ferromagnetic (FM) and antiferromagnetic (AFM) interactions lead to a very peculiar phase diagram characterized by reentrance phenomena. The system undergoes a paramagnetic (PM) phase to FM phase at a ferromagnetic critical temperature T_c, and a FM phase to a reentrant spin-glass (RSG) phase at a reentrant spin-glass transition temperature T_{RSG}.

Stage-2 $Cu_cCo_{1-c}Cl_2$ graphite intercalation compounds (GICs) are one of the reentrant ferromagnets.[6,7] The structure of these systems is characterized by a staging structure. The $Cu_cCo_{1-c}Cl_2$ intercalate layers sandwiched by adjacent graphene sheets are periodically stacked along the c axis. The $Cu_cCo_{1-c}Cl_2$ intercalate layer consists of Cu_cCo_{1-c} layers sandwiched by adjacent Cl layers. Because of the large separation distance between adjacent Cu_cCo_{1-c} layers, these systems magnetically behave like a quasi-two-dimensional (2D) random spin system. In each Cu_cCo_{1-c} layer Cu^{2+} and Co^{2+} ions are randomly distributed on the lattice sites. The spin frustration effect occurs as a result of the competition between the FM interactions (Co^{2+}-Co^{2+} and Co^{2+}-Cu^{2+}) and the AFM interaction (Cu^{2+}-Cu^{2+}). In a pure stage-2 $CuCl_2$ GIC ($c=1$) there is another type of spin frustration effect arising from the frustrated nature of the system: the antiferromagnet on the isosceles triangular lattice.[8]

The magnetic phase diagram of these systems depends on the Cu concentration. The system with $c \geq 0.4$ magnetically behaves like a reentrant ferromagnet (see Fig. 1 for the magnetic phase diagram).[6,7] The phase transitions occur at a RSG transition temperature (T_{RSG}) and a Curie temperature (T_c). The intermediate phase between T_c and T_{RSG} is the FM phase and the low temperature phase is the RSG phase. With further increasing the Cu concentration above $c=0.93$, the spin frustration effect is much more enhanced. Above a multicritical point c_{MCP} ($c_{MCP} \approx 0.96$), a FM long range order no longer exists. Only the spin glass phase survives for $c_{MCP} < c < 1$. For stage-2 $CuCl_2$ GIC ($c=1$), no phase transition occurs at least above $T=0.3$ K, mainly because of the frustrated nature of the 2D antiferromagnet on the isosceles triangular lattice.[8]

In the present paper, we report our experimental study on the magnetic phase transitions of reentrant ferromagnet, stage-2 $Cu_{0.93}Co_{0.07}Cl_2$ GIC ($T_{RSG}=6.64$ K and $T_c=8.62$ K) near $c=c_{MCP}$ where the PM-FM, FM-RSG, RSG-SG, and SG-PM boundaries merge. Because of the enhanced frustrated nature of the system, the FM phase may be very different from an ideal FM phase with long range order. It may be ferromagnetic chaotic phase with short range order.

The static and dynamic nature of the RSG and FM phases is extensively studied from the measurements of dc and ac magnetic susceptibility using a superconducting quantum interference device (SQUID) magnetometer. Our study in-

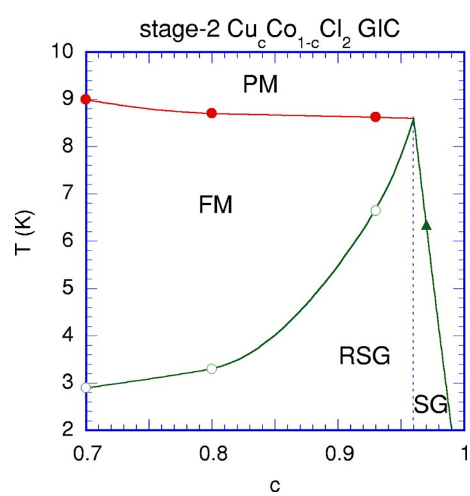

FIG. 1. (Color online) Magnetic phase diagram of stage-2 $Cu_cCo_{1-c}Cl_2$ GIC for $0.7 \leq c \leq 1$. The multicritical point is located at $c_{MCP} \approx 0.96$ and $T_{MCP} \approx 8.8$ K. The solid lines are guides to the eyes.

cludes the T dependence of nonlinear ac magnetic susceptibility, the memory phenomena of dc magnetization, the dynamic scaling relation of the absorption $\chi''(\omega,T)$, and the scaling plot of $\chi'(T,H)$ above T_c. Details of the aging dynamics of the present system will be presented elsewhere. For $0.4 \leq c \leq 0.8$, the absorption of the ac magnetic susceptibility χ'' clearly exhibits two peaks at T_{RSG} and T_c,[7] while for $c=0.93$, no peak in χ'' is observed at T_{RSG} (see Sec. III E). The existence of the RSG phase for $c=0.93$ is experimentally confirmed from the above methods.

II. EXPERIMENTAL PROCEDURE

The detail of the sample characterization of stage-2 $Cu_{0.93}Co_{0.07}Cl_2$ GIC was reported in our previous paper.[7] The stoichiometry of the system is given by $C_nCu_{0.93}Co_{0.07}Cl_2$ with $n=11.42$. Cu^{2+} and Co^{2+} ions are randomly distributed on the triangular lattice sites of the $Cu_{0.93}Co_{0.07}$ intercalate layer. The repeat distance between adjacent intercalate layers is $d=12.80\pm0.05$ Å. The dc magnetization and ac magnetic susceptibility were measured using a SQUID magnetometer (Quantum Design MPMS XL-5) with an ultralow field capability as an option. The detail of each experimental procedure will be described in Sec. III. The nonlinear ac magnetic susceptibility was measured as follows, where h is the amplitude of the ac field. After each h-scan (h $=1$ mOe to 4.2 Oe) at fixed T, T was increased by ΔT $=0.1$ K in the temperature range between 1.9 and 12.0 K. The nonlinear ac magnetic susceptibility was measured where $f=1$ Hz. The detail of the experimental procedure has been reported in our previous papers.[4,9] Experimentally, Θ_1' and Θ_1'' are the in-phase and out-of-phase components of the first harmonics of the ac magnetization:

$$\frac{\Theta_1'}{h} = \chi_1' + \frac{3}{4}\chi_3' h^2 + \frac{10}{16}\chi_5' h^4 + \frac{35}{64}\chi_7' h^6 + \cdots, \tag{1}$$

$$\frac{\Theta_1''}{h} = \chi_1'' + \frac{3}{4}\chi_3'' h^2 + \frac{10}{16}\chi_5'' h^4 + \frac{35}{64}\chi_7'' h^6 + \cdots. \tag{2}$$

The least-squares fits of the data (Θ_1'/h vs h and Θ_1''/h vs h) ($10\text{ mOe} \leq h \leq 4.2$ Oe) for each T yields the nonlinear susceptibility.

III. RESULT

A. T dependence of M_{ZFC}, M_{FC}, M_{TRM}, and ΔM ($=M_{FC}-M_{ZFC}$)

The measurements of M_{ZFC}, M_{FC}, and M_{TRM} were made as follows. (i) *The zero-field cooled magnetization* (M_{ZFC}) *measurement*. The system was annealed at 50 K for 1200 s in the absence of H. The system was cooled from 50 to 2 K at $H=0$ through the ZFC cooling protocol. After the system was aged at 2 K for $t_w=100$ s at $H=0$, the magnetic field is applied at H (=1 Oe) and subsequently M_{ZFC} was measured with increasing T from 2 to 12 K at the rate of 0.025 K/min. (ii) *The field cooled magnetization* (M_{FC}) *measurement*. The system was annealed at 50 K for 1200 s in the presence of H. Then the system was quenched from 50 to 12 K in the presence of H through the FC cooling protocol. The magnetization M_{FC} was measured with decreasing T from 12 to 2 K. (iii) *The thermoremnant magnetization* (M_{TRM}) *measurement*. The system was cooled from 50 to 2 K in the presence of H through the FC cooling protocol. After the system was aged at 2 K for $t_w=100$ s, the field was cutoff ($H=0$). Then the magnetization M_{TRM} was measured with increasing T from 2 to 12 K.

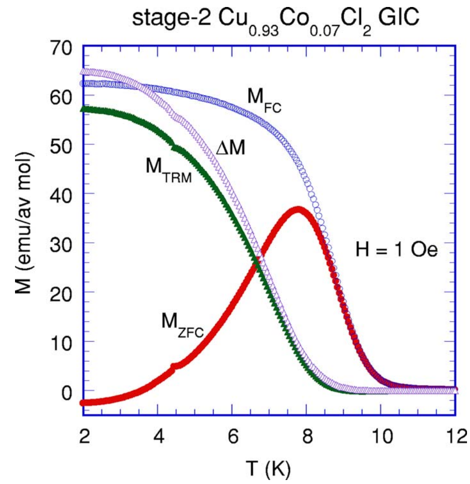

FIG. 2. (Color online) T dependence of M_{FC}, M_{ZFC}, ΔM ($=M_{FC}-M_{ZFC}$), and M_{TRM} at $H=1$ Oe. The effect of a remnant magnetic field (≈ 3 mOe) on magnetization curves is corrected by subtracting the magnetization in a remnant magnetic field (≈ 3 mOe) from magnetization data. The negative value of M_{ZFC} near 2 K may result from such a subtraction.

Figure 2 shows the T dependence of M_{ZFC}, M_{FC}, M_{TRM}, and $\Delta M=M_{FC}-M_{ZFC}$ at $H=1$ Oe. M_{ZFC} shows a peak at 7.75 K. The deviation of M_{ZFC} from M_{FC} starts to occur below about 9.8 K, which is rather higher than the peak temperature of χ_{ZFC}. The derivative dM_{FC}/dT at $H=1$ Oe shows a negative local minimum near T_c (=8.62 K), while the derivatives dM_{TRM}/dT and $d\Delta M/dT$ show a negative local minimum near T_{RSG} (=6.64 K). These results suggest that the system undergoes two magnetic phase transitions at T_{RSG} and T_c.

Similar experiments have been carried out at $H=5$ Oe. Both the derivatives dM_{TRM}/dT and $d\Delta M/dT$ exhibit a negative local minimum at $T_{RSG}(H=5\text{ Oe}) \approx 6$ K, which is indicative of the decrease of $T_{RSG}(H)$ with increasing H from $H=1$ to 5 Oe. In contrast, the derivative dM_{FC}/dT exhibits a local maximum at $T_c(H=5\text{ Oe})=8.8$ K, indicating a slight increase of $T_c(H)$ with increasing H from 1 to 5 Oe.

The aging dynamics of this system will be reported elsewhere.[10] Here we note that the relaxation rate $S(t)$ [$=d\chi_{ZFC}(t)/d\ln t$] exhibits a peak at a peak time t_{cr}. We find that the peak height of $S(t)$ at $t=t_{cr}$ shows a local maximum at T_{RSG}, but no anomaly at T_c.

B. Nonlinear ac magnetic susceptibility

Figure 3 shows the T dependence of the dispersion (Θ_1'/h) and the absorption (Θ_1''/h) of the ac magnetic suscep-

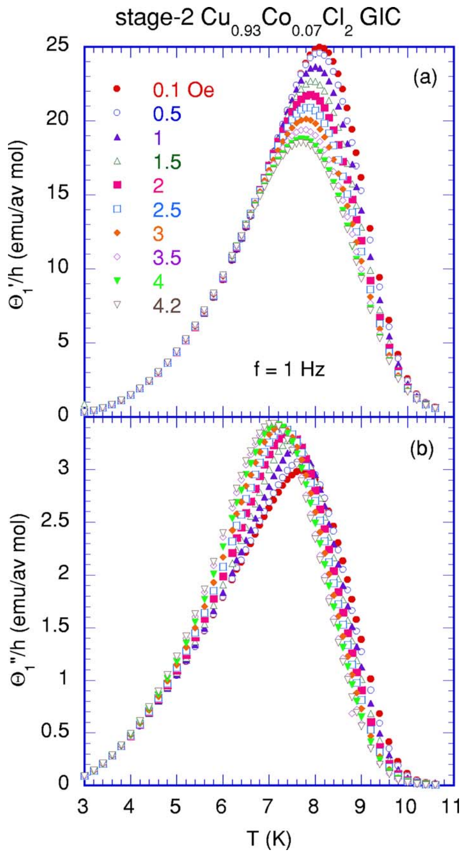

FIG. 3. (Color online) T dependence of (a) the dispersion Θ_1'/h and (b) the absorption Θ_1''/h at various h (=0.1–4.2 Oe). $H=0$. $f=1$ Hz.

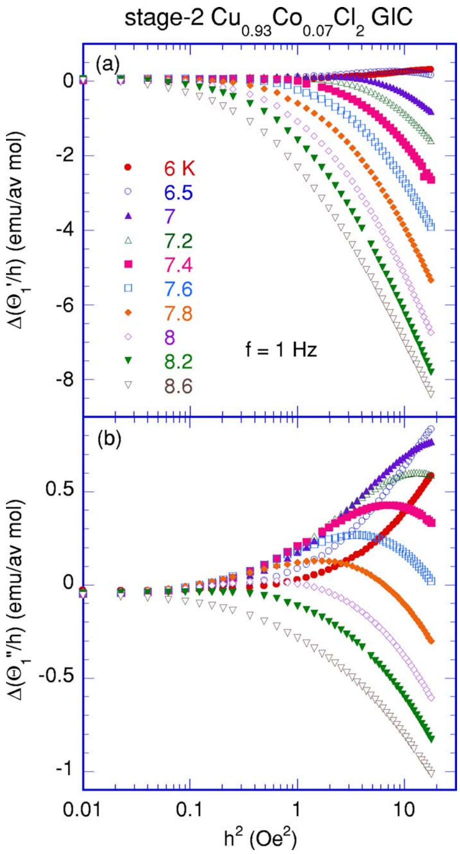

FIG. 4. (Color online) Plot of $\Delta(\Theta_1'/h)$ and $\Delta(\Theta_1''/h)$ as a function of h^2, where $\Delta(\Theta_1'/h)$ and $\Delta(\Theta_1''/h)$ are defined as the difference between Θ_1'/h and Θ_1''/h at h and those at $h=0.01$ Oe, respectively.

tibility, where $f=1$ Hz. The different curves correspond to different amplitude of the ac field, $0.1 \leq h \leq 4.2$ Oe. The features of Θ_1'/h vs T and Θ_1''/h vs T are summarized as follows. Both Θ_1'/h and Θ_1''/h exhibit a peak at a temperature between T_{RSG} and T_c. These peaks linearly shift to the low-T side with increasing the ac amplitude h. The curve of Θ_1'/h vs T is independent of h below 6 K, but it is strongly dependent on h at temperatures between 6 and 10 K even far above T_c. The curve of Θ_1''/h vs T is independent of h below 5 K but it is strongly dependent on h at temperatures between 5 and 10 K.

Both the FM phase and the RSG phase exhibit strong nonlinearities and slow dynamics. There is a characteristic ac field $h_0(T)$. For $h < h_0(T)$, both Θ_1'/h vs T and Θ_1''/h vs T do not depend on h below T_{RSG}, suggesting the linear response of the system. Here we discuss the nonlinear ac magnetic susceptibility. For convenience, we define $\Delta(\Theta_1'/h)$ and $\Delta(\Theta_1''/h)$ as the difference between Θ_1'/h and Θ_1''/h at h and those at $h=0.01$ Oe. Note that the data at $h=0.01$ Oe are the same as that at $h=0.1$ Oe shown in Fig. 3. Figures 4(a) and 4(b) show the plot of $\Delta(\Theta_1'/h)$ and $\Delta(\Theta_1''/h)$ as a function of h^2, respectively. Both $\Delta(\Theta_1'/h)$ and $\Delta(\Theta_1''/h)$ are strongly dependent on h^2 between T_c and T_{RSG}. Figures 5(a) and 5(b) show the T dependence of the nonlinear ac magnetic susceptibility $(\chi_3', \chi_5', \chi_7', \chi_3'', \chi_5'', \chi_7'')$ at $f=1$ Hz. The T dependence of χ_1' $(=\chi')$ and χ_1'' $(=\chi'')$ will be discussed in Sec. III E. The linear susceptibility (χ_1' and χ_1'') shows no change of sign, while the nonlinear ac susceptibility (χ_3', χ_5', χ_7', χ_3'', χ_5'', and χ_7'') undergoes several changes of sign between 6 and 10 K. The features of the T dependence of the linear and nonlinear ac susceptibilities are summarized as follows. The linear dispersion χ_1' exhibits a peak at 8.10 K. The nonlinear dispersion χ_3' starts to appear above $T=6.0$ K as T increases and exhibits a positive local maximum at T_{RSG} and a local negative minimum at T_c, which is much more pronounced compared with the positive local maximum. The nonlinear dispersion χ_5' shows a positive local maximum at 6.0 K, a zero crossing at 6.28 K ($<T_{RSG}$), a negative local minimum at 7.42 K, and a positive local maximum at T_c. The linear absorption χ_1'' has a peak at 7.75 K. The nonlinear absorption χ_3'' starts to appear above $T=5$ K with increasing T and exhibits a positive local maximum at 7.42 K between T_{RSG} and T_c and a negative local minimum around T_c.

It is predicted from the mean field theory that the nonlinear dc susceptibility χ_3 diverges on both sides of T_c for the PM-FM transition of the FM system.[11] The sign of χ_3 changes from a negative to a positive sign as T decreases and crosses T_c. On the other hand, χ_3 diverges negatively at T_{SG} for the PM-SG transition of the SG system.[12] As far as we know, there has been no theoretical prediction for χ_3 vs T for the FM-RSG transition. In our system, the sign of the local maximum in χ_3' at T_{RSG} is opposite to that of the local minimum in χ_3 at T_{SG} in the SG system. On the other hand the

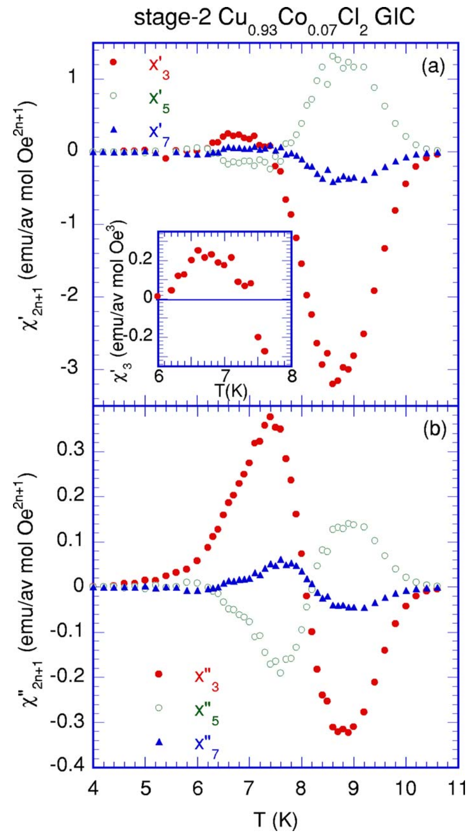

FIG. 5. (Color online) T dependence of the nonlinear ac susceptibility. $f=1$ Hz. (a) χ'_{2n+1} ($n=1$, 2, and 3) (the detail of χ'_3 vs T is shown in the inset) and (b) χ''_{2n+1} ($n=1$, 2, and 3).

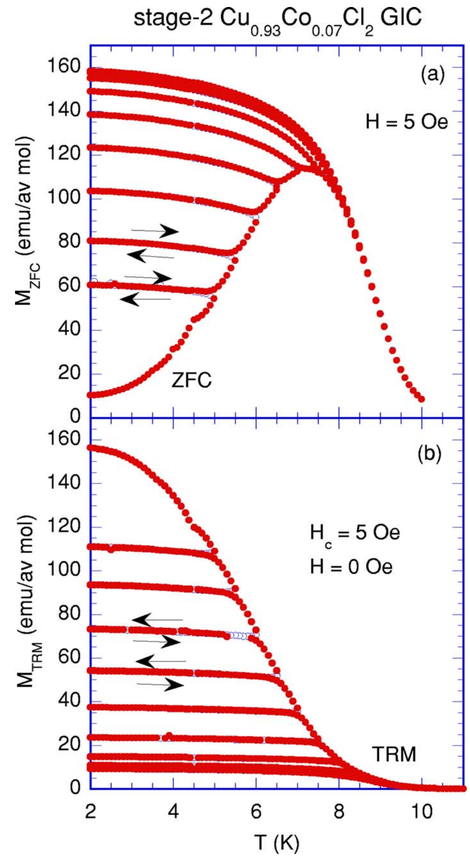

FIG. 6. (Color online) (a) T dependence of M_{ZFC} in a series of heating and cooling processes described in the text, after the ZFC cooling protocol from 50 to 2 K. $H=5$ Oe. (b) T dependence of M_{TRM} in a series of heating and cooling processes described in the text, after the FC cooling protocol from 50 to 2 K in the presence of $H_c=5$ Oe. $H=0$ during the measurement of M_{TRM}. The effect of the remnant field is corrected for each magnetization curve.

sign of the local minimum in χ'_3 at T_c is the same as that of the local minimum in χ_3 at T_c in the FM system. Here we note that similar phenomena are also observed in χ'_3 and χ''_3 for the reentrant ferromagnet $Ni_{77}Fe_1Mn_{22}$.[13] The nonlinear dispersion χ'_3 exhibits a negative local minimum at T_{RSG} and a positive local maximum at T_c. The nonlinear absorption χ''_3 exhibits only a negative local minimum at T_c. No anomaly in χ''_3 is observed. The sign of χ'_3 for $Ni_{77}Fe_1Mn_{22}$ is opposite to that of our system.

In summary, χ'_3 and χ''_3 of reentrant ferromagnets show complicated T dependence in the vicinity of T_{RSG} and T_c. The sign and the position of local minimum and local maximum are not sufficiently understood in terms of the simple mean field theory. This suggests that the T dependence of χ'_3 and χ''_3 provides a strong measure for the degree of frustrated nature of the systems near the multicritical point. Further discussion will be presented in Sec. IV D.

C. Memory phenomena in M_{ZFC} and M_{TRM}

We have measured two types of peculiar memory phenomena for ZFC and TRM magnetization, which have been found in stage-2 $CoCl_2$ GIC by Matsuura *et al.*[14] Here we present our result on memory phenomena of M_{ZFC} and M_{TRM} for stage-2 $Cu_{0.93}Co_{0.07}Cl_2$ GIC, which is observed in a series of heating and cooling processes. Such a characteristic phenomenon has been predicted theoretically in spin glass based on a successive bifurcation model of the energy level scheme below the spin freezing temperature.[15]

(i) *ZFC case*. Before the ZFC magnetization measurement, a ZFC protocol was carried out. It consists of the following processes: (a) annealing of the system at 50 K for 1200 s in the absence of H, (b) quenching of the system from 50 to 2 K, and (c) aging the system at $T_i=2$ K and $H=0$ for a wait time $t_w=100$ s. Just after the magnetic field ($H=5$ Oe) is applied to the system, the ZFC magnetization M_{ZFC} was measured with increasing T from T_i (=2 K) to T_1 (=5 K) and subsequently with decreasing T from T_1 to T_i. Next it was measured with increasing T from T_i to T_2 (=5.5 K) (the heating process) and subsequently with decreasing T from T_2 to T_i (the cooling process). This process was repeated for the U-turn temperatures T_r ($r=3-11$), where $T_r>T_i$, $\Delta T=T_{r+1}-T_r=0.5$ K, and $T_{11}=10.5$ K. Figure 6(a) shows a typical example of the T dependence of M_{ZFC} using the above method. Note that the value of M_{ZFC} lies between those of M_{ZFC}^{ref} and M_{FC}^{ref} at any T below T_c. Here M_{ZFC}^{ref} is measured with increasing T from T_i to 12 K at $H=5$ Oe after the ZFC cooling protocol. The magnetization M_{FC}^{ref} is measured with decreasing T from a temperature far above T_c to T_i in the presence of H (=5 Oe). For $T_r<T_{RSG}$,

the value of M_{ZFC} at T_i obtained after the cooling process ($T=T_r \rightarrow T_i$) is slightly larger than that at T_r before the cooling process. The path of M_{ZFC} vs T in the cooling process ($T=T_r \rightarrow T_i$) is exactly the same as that in the subsequent heating process ($T=T_i \rightarrow T_r$), indicating the reversibility of such a series of process. The spin configuration imprinted at T_r remains unchanged after the cooling and heating processes ($T=T_r \rightarrow T_i \rightarrow T_r$), indicating a memory phenomenon. Even for $T_{RSG} < T < T_c$, the path of M_{ZFC} vs T in the cooling process ($T=T_r \rightarrow T_i$) still coincides with that in the heating process ($T=T_i \rightarrow T_r$). For $T_i \geqslant T_c$, both the path of M_{ZFC} in the cooling process ($T=T_r \rightarrow T_i$) and path of M_{ZFC} in the heating process ($T=T_i \rightarrow T_r$) coincide with that of M_{FC}^{ref} which is obtained by cooling from the PM phase to $T=T_i$ in the presence of $H=5$ Oe.

(ii) *TRM case*. Before the TRM magnetization measurement, a field cooling (FC) protocol was carried out, consisting of (a) annealing of the system at 50 K for 1200 s in the presence of H (=5 Oe), (b) quenching of the system from 50 to 2 K, and (c) aging the system at $T=T_i=2$ K and $H=5$ Oe for a wait time $t_w=100$ s. Just after the magnetic field was turned off, the TRM magnetization was measured using the same procedure of heating and cooling: $T_i \rightarrow T_1 \rightarrow T_i \rightarrow T_2 \rightarrow T_i \rightarrow T_3 \rightarrow T_i \rightarrow$ and so on. Figure 6(b) shows a typical example of the T dependence of M_{TRM} using this method. The value of M_{TRM} lies between those of the M_{TRM}^{ref} and $M=0$ line at any T below T_c. Here the magnetization M_{TRM}^{ref} is measured with increasing T from T_i to 12 K at $H=0$ after the FC cooling protocol at a field $H_c=5$ Oe. For $T_r < T_{RSG}$, the value of M_{TRM} at T_i obtained after the cooling process ($T=T_r \rightarrow T_i$) is nearly equal to that at T_r. The path of M_{TRM} vs T in the cooling process ($T=T_r \rightarrow T_i$) coincides with that in the heating process ($T=T_i \rightarrow T_r$), indicating that the spin configuration at T_r is maintained during the cooling and heating process between T_r and T_i. Even for $T_{RSG} < T < T_c$, the path of M_{TRM} vs T in the cooling process ($T=T_r \rightarrow T_i$) is the same as that in the heating process ($T=T_i \rightarrow T_r$). For $T_r \geqslant T_c$, the path of M_{TRM} vs T in the cooling process ($T=T_r \rightarrow T_i$) is the same as that of M_{TRM} vs T in the heating process ($T=T_i \rightarrow T_r$). In fact, M_{TRM} in the cooling process ($T=T_r \rightarrow T_i$) corresponds to M_{FC} which is obtained from the FC cooling under a small remnant field (≈ 3 mOe) from the PM phase.

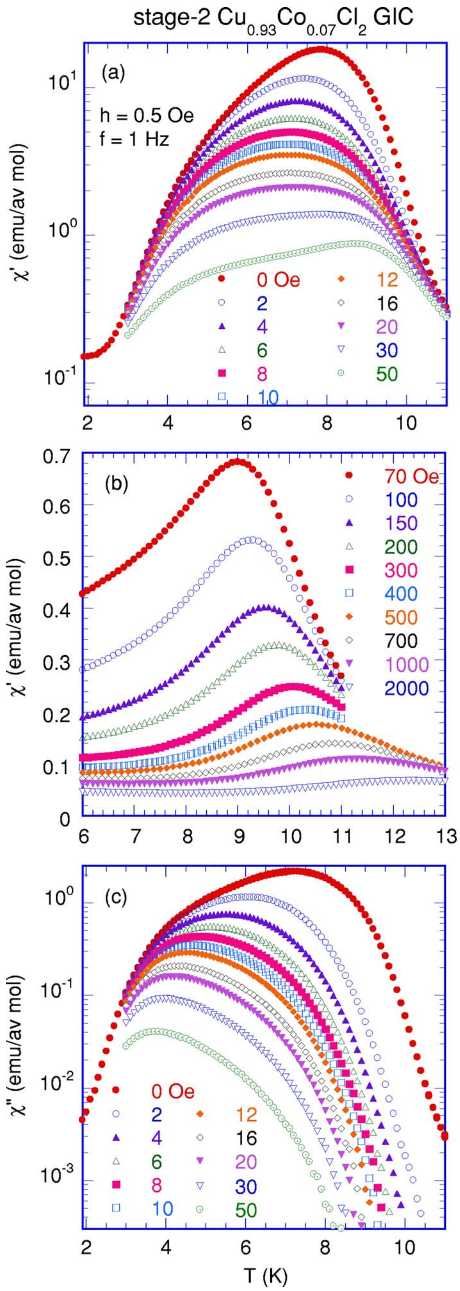

FIG. 7. (Color online) T dependence of (a) χ' for $0 \leqslant H \leqslant 50$ Oe, (b) χ' for $70 \leqslant H \leqslant 2000$ Oe, and (c) χ'' for $0 \leqslant H \leqslant 50$ Oe. $f=1$ Hz. $h=0.5$ Oe.

D. *H*-*T* phase diagram

1. χ' vs *T* and χ'' vs *T* in the presence of *H*

Figures 7(a)–7(c) show the T dependence of χ' and χ'' in the presence of H ($0 \leqslant H \leqslant 2500$ Oe), where $f=1$ Hz and $h=0.5$ Oe. The peak of χ' associated with the RSG transition shifts to the low-T side with increasing H for $0 \leqslant H \leqslant 10$ Oe. The peak height drastically decreases with increasing H. At $H=50$ Oe, a broad peak associated with the FM transition becomes pronounced around $T=T_c$ because of the strong suppression of the broad RSG peak in the presence of H. The peak associated with the FM phase shifts to the high-T side with increasing H above 100 Oe. In contrast, the peak of χ'' shifts to the low-T side with increasing H ($0 \leqslant H \leqslant 150$ Oe). The peak height drastically decreases with increasing H and reduces to zero above 150 Oe. Here we define $\chi'_{max}(H)$ and $T_{max}(H)$ as the peak height and the peak temperature of the FM-broad peak of $\chi'(T,H)$ vs T at the fixed H, respectively. Note that $T_{max}(H)$ is not a critical temperature except for $H=0$: $T_{max}(H=0)=T_c$. It is considered to be a temperature below which the magnetic-field induced ferromagnetic state appears. In Fig. 8, we show the H-T diagram. The peak temperatures of χ' and χ'' are plotted as a function of T, forming two lines denoted as $T_{RSG}(H)$ and $T_{max}(H)$. The temperature $T_{RSG}(H)$ decreases with increasing H, while $T_{max}(H)$ increases with increasing H. Similar be-

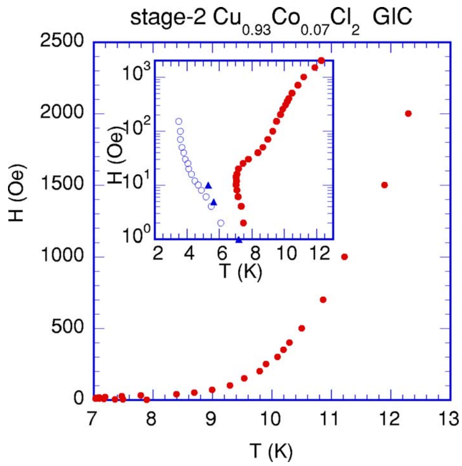

FIG. 8. (Color online) H-T diagram, where the peak temperatures of χ' vs T (●) and χ'' vs T (○) are plotted as a function of T. Negative local minimum temperatures of $d\Delta\chi/dT$ vs T (▲) are also plotted as a function of H. $\Delta\chi=\chi_{FC}-\chi_{ZFC}$.

havior in χ' above T_c in the presence of H has been observed in a 2D XY-like ferromagnet K_2CuF_4.[16] Using the same method used in K_2CuF_4, we examine the static scaling hypothesis for the dispersion $\chi'(T,H)$ above T_c in the presence of H. The dispersion $\chi'(T,H)$ is described by a scaling function,

$$\chi'(T,H)=\epsilon^{-\gamma}f(H/\epsilon^{\Delta})=(H/\epsilon^{\Delta})^{\gamma/\Delta}H^{-\gamma/\Delta}f(H/\epsilon^{\Delta})$$
$$=H^{-\gamma/\Delta}\psi(H/\epsilon^{\Delta}), \tag{3}$$

where $\epsilon=T/T_c-1$ and $f(H/\epsilon^{\Delta})$ and $\psi(H/\epsilon^{\Delta})=(H/\epsilon^{\Delta})^{\gamma/\Delta}\times f(H/\epsilon^{\Delta})$ are single-valued functions of H/ϵ^{Δ}. The critical exponent Δ is defined as $\Delta=\beta+\gamma$, where β and γ are critical exponents of magnetization and susceptibility. Figure 9(a) shows χ'_{max} as a function of H. The least-squares fit of the data of χ'_{max} vs H for 70 Oe$\leqslant H\leqslant$2 kOe to a power law form $\chi'_{max}\approx H^{-\gamma/\Delta}$ yields the exponent $\gamma/\Delta=0.689\pm0.001$. In Fig. 9(a) we also show the deviation ϵ_{max} $(=T_{max}/T_c-1)$ as a function of H, where $T_c=8.62$ K. The least-squares fit of the data to a power law form $H=H_0\epsilon_{max}^{\Delta}$ for 200 Oe$\leqslant H\leqslant$2 kOe yields the exponent $\Delta=2.03\pm0.03$ and $H_0=139\pm4$ Oe. Using the scaling relation, $\alpha+2\beta+\gamma=2$, we have $\alpha=-0.66$, $\beta=0.63$, and $\gamma=1.40$, where α is the critical exponent of the heat capacity. In Fig. 9(b) we show a scaling plot of $Y=\chi'(T,H)H^{\gamma/\Delta}$ as a function of $X=H/\epsilon^{\Delta}$, where all the data of $\chi'(T,H)$ vs T with fixed H (70 Oe$\leqslant H\leqslant$2 kOe) and $9.3\leqslant T\leqslant 14$ K) are plotted. Almost all the data points are well located on a scaling function which has a broad peak around $X=10^4$, indicating the validity of the static scaling hypothesis for the present system above T_c in an external magnetic field. The critical exponent obtained here will be discussed in Sec. IV C.

2. χ_{ZFC} vs T, χ_{FC} vs T, and $\Delta\chi$ vs T in the presence of H

Figures 10(a) and 10(b) show the T dependence of χ_{ZFC} and χ_{FC} in the presence of the fixed H ($H=5-600$ Oe). The susceptibility χ_{ZFC} shows a broad peak, which shifts to the low-T side with increasing H. Correspondingly, the peak

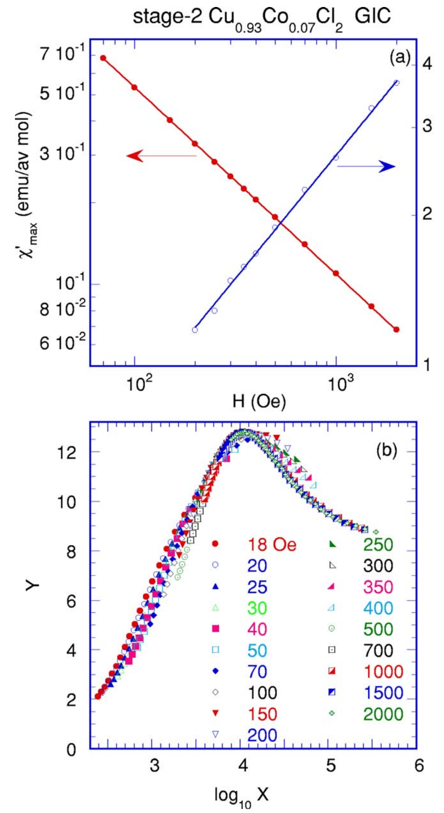

FIG. 9. (Color online) (a) H dependence of χ'_{max} and ϵ_{max} $(=T_{max}/T_c-1)$, where $T_c=8.62$ K. (b) Scaling plot of $Y=\chi'(T,H)H^{\gamma/\Delta}$ as a function of $X=H/\epsilon^{\Delta}$. $\epsilon=T/T_c-1$. $T_c=8.62$ K. $\Delta=2.03$. $9.3\leqslant T\leqslant 13.0$ K.

height becomes smaller and the peak width becomes broader. The deviation of χ_{ZFC} from χ_{FC} occurs below some characteristic temperature dependent on H. The susceptibility χ_{FC} is nearly temperature independent at the lowest T. These features are indicative of the existence of the RSG phase below $T_{RSG}(H)$. Here we define $\Delta\chi$ as the difference between χ_{FC} and χ_{ZFC}: $\Delta\chi=\chi_{FC}-\chi_{ZFC}$, which provides a measure for the irreversibility of susceptibility. The difference $\Delta\chi$ drastically decreases with increasing T. The RSG transition temperature $T_{RSG}(H)$ is usually defined as a temperature at which $\Delta\chi$ is equal to zero. However, it is a little difficult to determine the transition temperature from this definition for the present system. For convenience, we define the RSG transition temperature at which the derivative $d\Delta\chi/dT$ has a negative local minimum. The derivative $d\Delta\chi/dT$ exhibits a local minimum at $H=1$, 5, and 10 Oe. The temperature for the negative local minimum drastically decreases with increasing T. The data thus obtained are plotted in the H-T diagram (see the inset of Fig. 8). These data points are located near the line for the H vs T_{RSG} where the peak temperatures of $\chi''(T,H)$ ($f=1$ Hz and $h=0.5$ Oe) are plotted as a function of H.

3. AT-like transition with an exponent p (=3/2)

Figure 10(c) shows the H-T diagram where the peak temperature of χ_{ZFC} is plotted as a function of H. This peak temperature at low H is a little higher than T_{RSG} (=6.64 K).

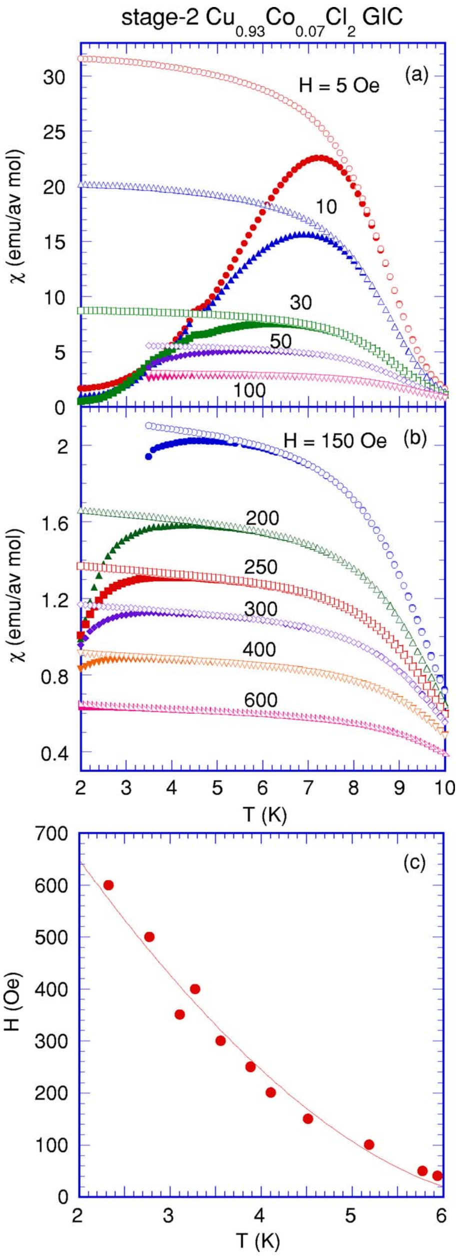

FIG. 10. (Color online) (a) and (b) T dependence of χ_{FC} and χ_{ZFC}. $5 \leq H \leq 600$ Oe. The effect of remnant field is corrected on each magnetization curve. (c) The H-T diagram, where the peak temperatures of χ_{ZFC} vs T are plotted as a function of H.

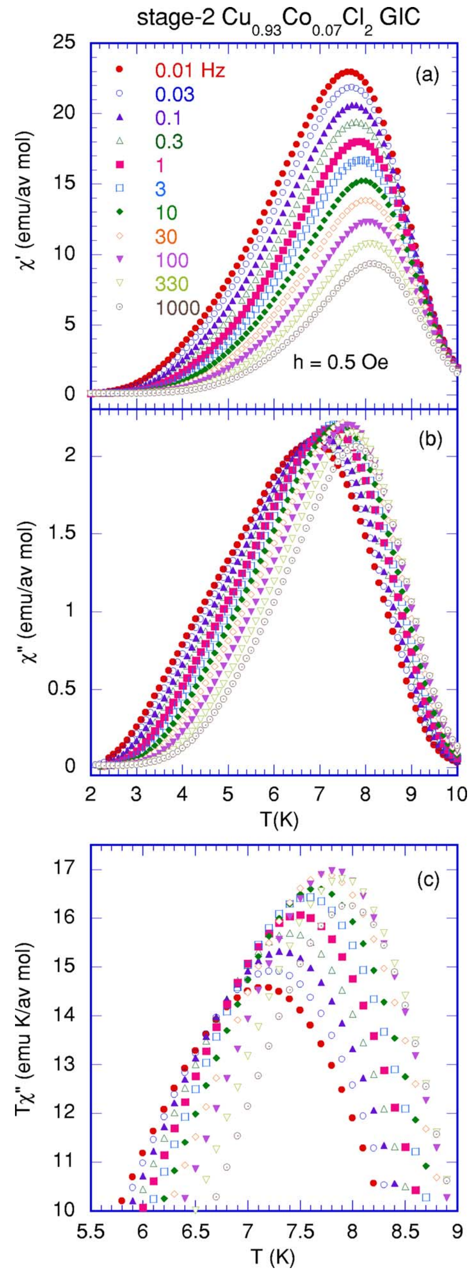

FIG. 11. (Color online) T dependence of (a) χ' and (b) χ'' at various f. $0.01 \leq f \leq 1000$ Hz. $h=0.5$ Oe. $H=0$ Oe. (c) T dependence of $T\chi''(\omega,T)$ at various f ($0.01 \leq f \leq 1000$ Hz). $h=0.5$ Oe. $H=0$ Oe.

The least-squares fit of the data(H vs T) in the limited temperature range ($2.3 \leq T \leq 6$ K) to a power law form

$$H = H_0^*\left(1 - \frac{T}{T_{RSG}}\right)^p, \tag{4}$$

yields the exponent $p=1.57\pm0.12$ and a magnetic field $H_0^*=1.16\pm0.11$ kOe, where T_{RSG} is fixed as $T_{RSG}=6.64$ K. The value of the exponent p is close to a de Almeida and Thouless (AT) value: $p=3/2$.[17] This result indicates the SG-like nature of RSG phase for the transition at T_{RSG}. Note that in the droplet picture[18] the SG transition can be destroyed in the absence of H. In fact, this picture is experimentally supported for $Fe_{0.5}Mn_{0.5}TiO_3$ (Ref. [19]) and $Cu_{0.5}Co_{0.5}Cl_2$–$FeCl_3$ graphite bi-intercalation compound (GBIC).[20]

E. f and T dependence of χ' and χ''

Figures 11(a) and 11(b) show the T dependence of the dispersion $\chi'(\omega,T)$ and the absorption $\chi''(\omega,T)$ at various f ($0.01 \leq f \leq 1000$ Hz). Since we use the ac field with $h=0.5$ Oe, we have $\chi' \approx \chi_1'$ and $\chi'' \approx \chi_1''$. The absorption χ'' exhibits a peak at $T=6.66$ K for $f=0.01$ Hz, while the dispersion χ' exhibits a peak at $T=7.65$ K for $f=0.01$ Hz. The derivative $\partial\chi''(\omega,T)/\partial T$ has a negative local minimum at

$T=8.48$ K, which corresponds to the temperature of the inflection point. Note that this inflection point does not coincide with the peak temperature of $\chi'(\omega,T)$. Both peaks of $\chi'(\omega,T)$ and $\chi''(\omega,T)$ shift to high-T side with increasing f.

In Fig. 11(c) we make a plot of $T\chi''(\omega,T)$ as a function of T. The peak of the curve of $T\chi''(\omega,T)$ vs T shifts to the high-T side with increasing f. The peak height increases with increasing f in the limited frequency range ($0.01 \leqslant f \leqslant 10$ Hz). Here we assume that $T\chi''(\omega,T)$ can be described by a dynamic scaling law above T_{RSG};[21]

$$T\chi''(\omega,T) = \epsilon^{\beta_{RSG}} G(\omega\tau) = \left(\frac{\omega\tau}{\tau_0^*}\right)^{-\beta_{RSG}/x} \omega^{\beta_{RSG}/x} G(\omega\tau) \approx \omega^{\beta_{RSG}/x} g(\omega\tau), \tag{5}$$

where ω ($=2\pi f$) is the angular frequency, β_{RSG} is a critical exponent, and $G(\zeta)$ and $g(\zeta)$ with $\zeta=\omega\tau$ are scaling functions

$$G(\zeta) = \zeta^{\beta_{RSG}/x} g(\zeta). \tag{6}$$

The relaxation time τ diverges on approaching T_{RSG} from the high-T side (a conventional critical slowing down),

$$\tau = \tau_0^* \epsilon^{-x}, \tag{7}$$

where τ_0^* is a microscopic relaxation time, $\epsilon=T/T_{RSG}-1$, $x=\nu z$, z is a dynamic critical exponent, and ν is the exponent for the spin correlation length. For simplicity, we assume that the scaling function $g(\omega\tau)$ has a peak at $\omega\tau=1$. In other words, it follows that $T\chi''(\omega,T)/\omega^{\beta_{RSG}/x}$ exhibits a peak at the peak temperature at which $\omega\tau=1$. Figure 12(a) shows the peak height of the data of $T\chi''(\omega,T)$ vs T, denoted as $[T\chi''(\omega,T)]_{max}$, as a function of f. The peak height increases with increasing f for $0.01 \leqslant f \leqslant 100$ Hz, showing a local maximum at $f=100$ Hz, and decreases with further increasing f. The least-squares fit of the data ($[T\chi''(\omega,T)]_{max}$ vs f) to a power law form ($\omega^{\beta_{RSG}/x}$) for $0.01 \leqslant f \leqslant 10$ Hz yields the exponent $\beta_{RSG}/x=0.0199\pm0.0004$. This value of β_{RSG}/x is much smaller than that ($=0.071\pm0.005$) reported for the reentrant Ising spin-glass $Fe_{0.62}Mn_{0.38}TiO_3$.[1] Figure 12(b) shows the T dependence of the relaxation time τ, where $\tau=1/\omega$ and T is the peak temperature of $T\chi''(\omega,T)$ vs T. The relaxation time τ drastically increases with decreasing T. The least-squares fit of the limited data of τ vs T for $0.01 \leqslant f \leqslant 10$ Hz and $6.8 \leqslant T \leqslant 8$ K to Eq. (7) yields the parameters $T_{RSG}=6.64\pm0.05$ K, $x=13.1\pm0.4$, and $\tau_0^*=(2.5\pm0.5)\times10^{-13}$ s. In Fig. 12(b) we show the plot of $\log_{10}(\tau)$ vs $\log_{10}(T/T_{RSG}-1)$ with $T_{RSG}=6.64$ K, where the solid line denotes the best-fit line. The value of x in the present system is very close to that of a reentrant Ising spin-glass $Fe_{0.62}Mn_{0.38}TiO_3$ ($x=13\pm2$).[1] Thus the transition from the FM phase to the RSG phase is dynamically similar to an ordinary transition from the PM phase to the SG phase in spin-glass systems. The critical exponent β_{RSG} is estimated as $\beta_{RSG}=0.25\pm0.02$. This value of β_{RSG} is smaller than those of β_{RSG} for the reentrant ferromagnet $Cu_{0.2}Co_{0.8}Cl_2$-$FeCl_3$ GBIC ($\beta_{RSG}=0.57$) (Ref. 5) and β_{SG} for the 3D Ising spin-glass $Cu_{0.5}Co_{0.5}Cl_2$-$FeCl_3$ GBIC ($\beta_{SG}=0.36\pm0.04$).[22]

In summary, the feature of the RSG-FM transition for stage-2 $Co_{0.93}Co_{0.07}Cl_2$ GIC is characterized by small β_{RSG} ($=0.25$) and the divergence of the relaxation time obeying a power law form given by Eq. (7) with large x ($=13.1$), $\tau_0^*=(2.5\pm0.5)\times10^{-13}$ s, and $T_{RSG}=6.64$ K.

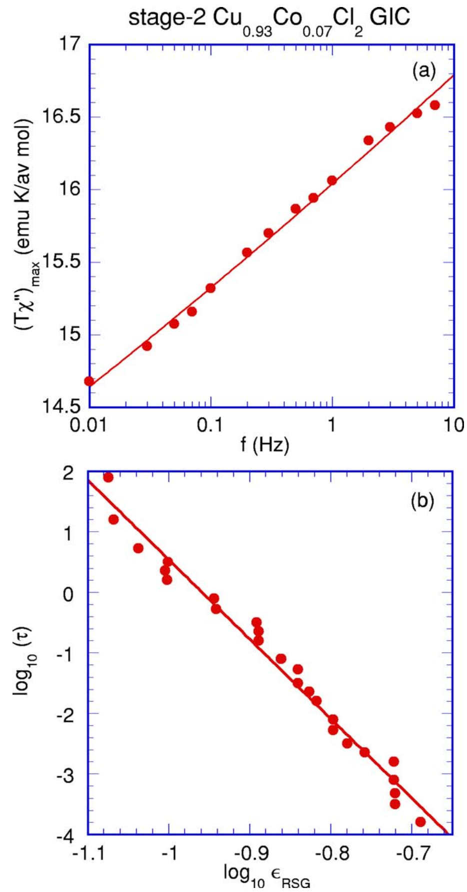

FIG. 12. (Color online) (a) Peak height of the data of $T\chi''(\omega,T)$ vs T, denoted as $[T\chi''(\omega,T)]_{max}$ as a function of f. $0.01 \leqslant f \leqslant 10$ Hz. (b) Plot of $\log_{10}\tau$ vs $\log_{10}\epsilon_{RSG}$ for $T\chi''(\omega,T)$ vs T. $\epsilon_{RSG}=T/T_{RSG}-1$. $6.8 \leqslant T \leqslant 8.0$ K. $T_{RSG}=6.64$ K. The solid lines denote least-squares fitting curves. The fitting parameters are given in the text.

F. f dependence of $\chi'(\omega,T)$ and $\chi''(\omega,T)$ vs T at fixed T

Figures 13(a) and 13(b) show the f dependence of $\chi'(\omega,T)$ and $\chi''(\omega,T)$ at fixed T, where $0.01 \leqslant f \leqslant 1000$ Hz and $h=0.5$ Oe. The absorption $\chi''(\omega,T)$ curves exhibit different characteristics depending on T. For $T \leqslant 6.4$ K, $\chi''(\omega,T)$ decreases with increasing f. For $6.5 \leqslant T \leqslant 8.0$ K, $\chi''(\omega,T)$ shows a peak at a characteristic frequency, shifting to the low-f side as T decreases. For $T \geqslant 8.1$ K $\chi''(\omega,T)$ decreases with increasing f. It is predicted from the scaling law given by Eq. (5) that the ω dependence of $\chi''(\omega,T)/\chi''_{max}$ at the fixed T coincides with that of the scaling function $G(\omega\tau)$ itself, where χ''_{max} is the maximum of $\chi''(\omega,T)$ vs f at the fixed T. In contrast, $\chi'(\omega,T)$ decreases with increasing f at any T.

We find that $\chi'(\omega,T)$ ($1.9 \leqslant T \leqslant 10.6$ K) is well described by a power law form,

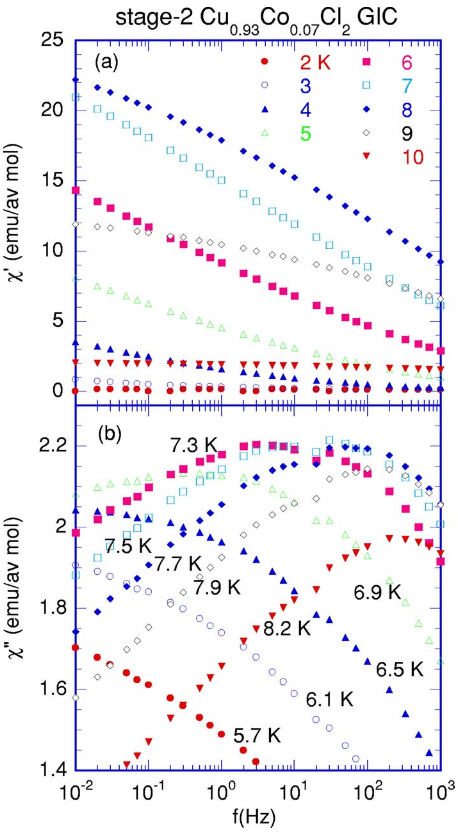

FIG. 13. (Color online) f dependence of (a) χ' and (b) χ'' at various T. h=0.5 Oe. H=0 Oe.

$$\chi'(\omega,T) \approx \omega^{a'} \tag{8}$$

in the frequency range $(0.01 \leqslant f \leqslant 10\ \text{Hz})$, where a' is the temperature-dependent exponent. The exponent a' is negative for any T and exhibits a negative local minimum around 3 K. It increases with increasing T: $a' \approx -0.07$ at $T=T_{RSG}$ and $a' \approx -0.03$ at $T=T_c$. The absorption $\chi''(\omega,T)$ is related to $\chi'(\omega,T)$ by a so-called $\pi/2$ rule[23]

$$\chi''(\omega,T) = -\frac{\pi}{2}\frac{\partial \chi'(\omega,T)}{\partial \ln \omega}, \tag{9}$$

which leads to the relation $a'=a''$, where a'' is the temperature-dependent exponent for $\chi''(\omega,T)$. According to the fluctuation and dissipation theorem, the magnetic noise power $S(\omega,T)$ is related to $\chi''(\omega,T)$ by[24]

$$S(\omega,T) = 4k_B T\frac{\chi''(\omega,T)}{\omega} \approx \omega^{-1+a''} \approx \omega^{-1+a'}, \tag{10}$$

where k_B is the Boltzmann constant. The magnetic noise power is proportional to $\omega^{-1.07}$ at $T=T_{RSG}$ and $\omega^{-1.03}$ at $T=T_c$. It follows a $1/f$-like behavior which is expected in SG systems.

IV. DISCUSSION

A. Ferromagnetic exchange interaction between Cu^{2+} and Co^{2+}

First we show that the intraplanar exchange interaction J(Co-Cu) between the nearest-neighbor pairs of Cu^{2+} and Co^{2+} ions should be ferromagnetic. To this end, we have measured the T dependence of χ_{FC} at H=1 kOe for the present system (c=0.93). The magnetic susceptibility for $150 \leqslant T \leqslant 300$ K obeys a Curie-Weiss law with the effective magnetic moment $P_{eff}(c=0.93)=2.42\pm0.03\ \mu_B$ and the Curie-Weiss temperature $\Theta(c=0.93)=-38.22\pm3.10$ K. According to the molecular field theory, the Curie-Weiss temperature $\Theta(c)$ for stage-2 $Cu_cCo_{1-c}Cl_2$ GIC can be expressed by[7]

$$\Theta(c) = \frac{c^2P_{eff}^2(1)\Theta(1) + (1-c)^2P_{eff}^2(0)\Theta(0) + 2\varepsilon c(1-c)\sqrt{|\Theta(1)\Theta(0)|}P_{eff}(1)P_{eff}(0)}{cP_{eff}^2(1)+(1-c)P_{eff}^2(0)}, \tag{11}$$

respectively, where $\Theta(0)=23.2$ K and $P_{eff}(0)=5.54\mu_B$ for stage-2 $CoCl_2$ GIC and $\Theta(1)=-100.9$ K, $P_{eff}(1)=2.26\mu_B$ for stage-2 $CuCl_2$ GIC.[8] The exchange interaction J(Cu-Co) may be expressed by a form

$$J(\text{Cu-Co}) = \varepsilon\sqrt{|J(\text{Cu-Cu})J(\text{Co-Co})|}, \tag{12}$$

where J(Co-Co) $[=\Theta(0)/3=7.73\ \text{K}]$ and J(Cu-Cu) $[=\Theta(1)/3=-33.63\ \text{K}]$ are the intraplanar exchange interactions between the nearest-neighbor $(Cu^{2+}-Cu^{2+})$ ion pairs and $(Co^{2+}-Co^{2+})$ ion pairs, respectively, and ε is only a parameter to be determined. From Eq. (11) with c=0.93 and $\Theta(c=0.93)=-38.22\pm3.10$ K, the parameter ε can be uniquely determined as $\varepsilon=2.26\pm0.02$, which leads to J(Cu-Co)=36.50 K. Note that the magnitude of FM interaction J(Cu-Co) is almost the same as that of AFM interaction J(Cu-Cu). This result suggests that the competition between mainly these two interactions gives rise to the spin frustration effect at c=0.93, forming a model equivalent to the $\pm J$ spin-glass model. The sign of $\Theta(c)$ changes at c_0=0.848 from positive to negative with increasing Cu concentration. This Cu concentration c_0 is a little smaller than c_{MCP} ($\approx$0.96).

B. Magnetic phase diagram (c vs T)

It has been theoretically predicted that the spin frustration plays an important role in 2D antiferromagnets on the triangular lattice (AFT). The phase transition of the AFT model depends on the nature of the spin symmetry. When interactions are restricted to nearest-neighbor spins, the AFT Ising model shows no phase transition at any temperature because of a degeneracy of the ground state caused by spin frustration.[25] For Heisenberg symmetry,[26] the AFT model predicts a more complex phase transition, driven by the dissociation of pairs of vortices formed of chirality vectors.

The stage-2 $CuCl_2$ GIC ($c=1$) magnetically behaves like a quasi-2D Heisenberg-like antiferromagnet ($S=1/2$) on the isosceles triangular lattice. Because of the fully frustrated nature of the system, no magnetic phase transition is observed at least above 0.3 K.[8] In the weak dilution limit ($c\approx 1$), there occurs another type of spin frustration effect due to the competition between the FM interaction J(Cu-Co) and the AFM interaction J(Cu-Cu), in addition to the spin frustration effect of the 2D AFT type.

These spin frustration effects lead to a complicated magnetic phase diagram (c vs T). For $c=0.97$ a SG phase appears below $T_{SG}=6.35$ K. For $c=0.93$, the system undergoes two magnetic phase transitions at T_{RSG} (=6.64 K) and T_c(=8.62 K). The magnetic phase diagram for $c\geqslant 0.4$ consists of the PM, RSG, FM, and SG phases. The PM-FM line, the FM-RSG line, and the SG-PM line intersect a multicritical point (MCP) at (c_{MCP},T_{MCP}), where $c_{MCP}\approx 0.96$ and $T_{MCP}=8.8$ K. Near the MCP point ($c<c_{MPC}$), there is a subtle interplay between the FM long range order and the random disorder and spin frustration of the RSG phase. At the present stage, the nature of the SG phase for $c_{MCP}<c<1$ has not been sufficiently examined yet. The shift in the MCP toward the Cu-rich end is the result of the ferromagnetic Cu-Co interaction. If one of the Co^{2+} and Cu^{2+} ions is nonmagnetic, the critical temperature reduces to zero at the percolation threshold concentration ($c_p=0.5$) for the 2D triangular lattice. In fact, in stage-2 $Co_cMg_{1-c}Cl_2$ GIC[27] where Mg is nonmagnetic, the transition temperature associated with the PM-FM transition tends to reduce to zero at $c\approx 0.5$.

C. Anomaly in critical exponent α associated with the PM-FM transition

We discuss the critical exponents of the reentrant ferromagnets near the MCP along the PM-FM line. As the concentration approaches the MCP, T_c becomes closer to T_{RSG} from the higher-T side. It is considered that the critical behavior near the PM-FM transition temperature T_c is strongly influenced by the random disorder and spin frustration. In fact, we show that the critical behavior of our system at T_c (=8.62 K) is characterized by the critical exponents $\alpha=-0.66$, $\beta=0.63$, and $\gamma=1.40$. These critical exponents are rather different from those predicted from the conventional models (2D Ising and XY models and the 3D Ising and XY models). The exponent γ of our system ($\gamma=1.40$) is close to that for the 3D Heisenberg ferromagnet ($\alpha=-0.1336$, $\beta=0.3689$, $\gamma=1.3960$, and $\nu=0.7112$),[28] while the critical exponents α and β are rather close to those of the 3D spherical model ($\alpha=-1$, $\beta=0.5$, $\gamma=2$, and $\delta=5$).[29]

Similar critical behavior at $T=T_c$ has been observed in several reentrant ferromagnets near the MCP. Yeshurun *et al.*[30] have studied the critical behavior of amorphous reentrant ferromagnet $(Fe_{1-c}Mn_c)_{75}P_{16}B_6Al_3$ at $c=0.32$ ($c_{MCP}=0.36$) along the PM-FM line: $\beta=0.40\pm 0.03$, and $\delta=5.3\pm 0.3$, where $T_c=100$ K and $T_{RSG}=38$ K. Using the scaling relations $\alpha+2\beta+\gamma=2$ and $\delta=(\beta+\gamma)/\beta$, the exponents α and γ are calculated as $\alpha=-0.52$ and $\gamma=1.72$. Yeshurun *et al.*[30] have also reported the critical exponents of the reentrant ferromagnet $(Fe_{1-c}Ni_c)_{75}P_{16}B_6Al_3$ at $c=0.80$ ($c_{MCP}=0.83$) along the PM-FM line at the PM-FM transition; $\alpha=-0.4$, $\beta=0.40\pm 0.04$, $\gamma=1.6$, and $\delta=5.0\pm 0.4$, where $T_c=90$ K and $T_{RSG}=21$ K. Pouget *et al.*[31] have examined the critical exponents of the reentrant ferromagnet $CdCr_{(2-2c)}In_{(2c)}S_4$ at $c=0.05$ ($c_{MCP}=0.15$), $T_c=68.5$ K, and $T_{RSG}=10.8$ K. The system with $c=0$ is a 3D Heisenberg ferromagnet. The critical exponents ($\alpha=-0.01$, $\beta=0.32$, $\gamma=1.37$, and $\nu=0.70$) are compatible with those for the 3D Heisenberg ferromagnet. A drastic change in the critical exponents is observed for the diluted system with $c=0.05$ ($\alpha=-0.57$, $\beta=0.30$, $\gamma=1.97$).

Thus it may be concluded from the above results that a negative large value of the heat capacity exponent α (=−0.4 to −0.66) is a feature common to the critical behavior of reentrant ferromagnets near the MPC. In our case, the pure system ($c=1$) belongs to the universality class of the 3D Heisenberg model ($\alpha=-0.1336$) in spite of no phase transition. The heat capacity exponent of our system with $c=0.93$ is a weakly diluted random system, where only 7% of Cu^{2+} ions are randomly replaced by Co^{2+} ions. It seems that our result violates the so-called Harris criterion.[32] According to this criterion, the dilution should be relevant only if the specific heat exponent α of the pure system is positive. In contrast, when $\alpha<0$, the dilution does not affect the critical behavior. In other words, the critical exponent of the diluted Heisenberg system is the same as that of the pure Heisenberg system. The Harris criterion may not be valid for the systems with competing exchange interactions, where the degree of disorder and spin frustration are greatly enhanced by the dilution. This result is consistent with the flow diagram of the renormalization group theory in the (c,T) plane.[33] For the dilution of a Heisenberg ferromagnet with no competing interactions, the renormalization group flow at the PM-FM critical line always ends at the critical point of the pure system ($c=1$). In the case of competing interactions, the renormalization group flow always ends at a new fixed point at the critical line.

D. Nonlinear susceptibility near the MCP

We show that the T dependence of the nonlinear ac susceptibility of our system near the MCP system is much more complicated than we expect. The nonlinear dispersion χ_3' for $f=1$ Hz is characterized by the zero value below 6 K, a local positive maximum at T_{RSG} (=6.64 K), the change of sign from positive to negative around 7.4 K with increasing T, and a local negative minimum at T_c. The local negative maximum at T_c is much more pronounced than the positive local maximum at T_{RSG}.

Here it is interesting to compare our results of χ_3' vs T with those of χ_3 vs T for the reentrant ferromagnet $(Fe_{1-c}Mn_c)_{75}P_{16}B_6Al_3$ with $c=0.26$, 0.30, and 0.32 near the

MCP ($c_{MPT}=0.36$), which have been reported by Berndt *et al.*[34,35] These systems undergo two transitions at T_c and T_{RSG}. For $c=0.26$, the nonlinear dc susceptibility χ_3 has a single negative local minimum at T_c. No anomaly is observed at T_{RSG}. For $c=0.30$, χ_3 consists of a less pronounced negative local minimum at T_{RSG} and a pronounced negative local minimum at T_c. In contrast, for $c=0.32$, the strength of these anomalies is reversed. The nonlinear susceptibility χ_3 consists of a pronounced negative local minimum at T_{RSG} and a less pronounced negative local minimum at T_c. These results indicate that as the concentration c approaches c_{MPC} from the low-c side, the contribution of the FM-RSG transition at T_{RSG} to χ_3 is more significant than that of the PM-FM transition at T_c to χ_3. Our result of χ_3' for $f=1$ Hz is qualitatively similar to those for $c=0.30$, except for the difference in the sign of the anomalies of χ_3 and χ_3' around T_{RSG}.

V. CONCLUSION

We show that stage-2 $Cu_{0.93}Co_{0.07}Cl_2$ GIC undergoes two magnetic phase transitions at T_{RSG} (=6.64±0.05 K) and T_c (=8.62±0.05 K). The static and dynamic nature of the RSG and FM phases has been extensively studied using various techniques. The nonlinear ac susceptibility χ_3' has a positive local maximum at T_{RSG}, and a negative local minimum at T_c. Peculiar memory phenomena for the ZFC and TRM magnetization are observed around T_{RSG} and T_c. The relaxation time τ between T_{RSG} and T_c shows a critical slowing down: $\tau=\tau_0^*(T/T_{RSG}-1)^{-x}$ with $x=13.1\pm0.4$ and $\tau_0^*=(2.5\pm0.5)\times10^{-13}$ s. The critical exponent β_{RSG} for the RSG phase is 0.25 ± 0.02, which is much smaller than that predicted for the SG phase. The influence of the random disorder on the critical behavior above T_c is clearly observed: $\alpha=-0.66$, $\beta=0.63$, and $\gamma=1.40$. The exponents of α and β are close to those of the 3D spherical model. The critical temperature $T_{RSG}(H)$ decreases with increasing temperature according to power law form given by Eq. (4) with the exponent $p=1.57\pm0.12$. This value of p is close to $p=3/2$ predicted by de Almeida and Thouless.

ACKNOWLEDGMENTS

The authors are grateful to H. Suematsu for providing single crystal of kish graphite and M. Matsuura for invaluable discussions. They would like to thank M. Johnson, B. Olson, T. Shima, C. Vartuli, and T.-Yu Huang for the sample preparation and characterization by using x-ray diffraction.

*Electronic address: itsuko@binghamton.edu
†Electronic address: suzuki@binghamton.edu

[1] K. Gunnarsson, P. Svedlindh, J.-O. Andersson, P. Nordblad, L. Lundgren, H. Aruga Katori, and A. Ito, Phys. Rev. B **46**, 8227 (1992).
[2] K. Jonason, J. Mattsson, and P. Nordblad, Phys. Rev. Lett. **77**, 2562 (1996).
[3] K. Jonason, J. Mattsson, and P. Nordblad, Phys. Rev. B **53**, 6507 (1996).
[4] M. Suzuki and I. S. Suzuki, Phys. Rev. B **69**, 144424 (2004), and references therein.
[5] M. Suzuki and I. S. Suzuki, Phys. Rev. B **71**, 174437 (2005), and references therein.
[6] I. S. Suzuki and M. Suzuki, Solid State Commun. **106**, 513 (1998).
[7] I. S. Suzuki and M. Suzuki, J. Phys.: Condens. Matter **11**, 521 (1999).
[8] M. Suzuki, I. S. Suzuki, C. R. Burr, D. G. Wiesler, N. Rosov, and K. Koga, Phys. Rev. B **50**, 9188 (1994).
[9] M. Suzuki, I. S. Suzuki, and T.-Yu Huang, J. Phys.: Condens. Matter **14**, 5583 (2002).
[10] M. Suzuki and I. S. Suzuki (unpublished).
[11] S. Chikazawa, C. J. Sandberg, and Y. Miyako, J. Phys. Soc. Jpn. **50**, 2884 (1981), and references therein.
[12] Masuo Suzuki, Prog. Theor. Phys. **58**, 1151 (1977).
[13] T. Sato, T. Ando, T. Ogawa, S. Morimoto, and A. Ito, Phys. Rev. B **64**, 184432 (2001).
[14] M. Matsuura, Y. Karaki, T. Yonezawa, and M. Suzuki, Jpn. J. Appl. Phys., Suppl. **26–S3**, 773 (1987).
[15] M. Matsuura, N. Tanaka, Y. Karaki, and Y. Murakami, Jpn. J. Appl. Phys., Suppl. **26-S3**, 797 (1987).
[16] M. Suzuki and H. Ikeda, J. Phys. Soc. Jpn. **50**, 1133 (1981).
[17] J. R. L. de Almeida and D. J. Thouless, J. Phys. A **11**, 983 (1978).
[18] D. S. Fisher and D. A. Huse, Phys. Rev. B **38**, 373 (1988); **38**, 386 (1988).
[19] J. Mattsson, T. Jonsson, P. Nordblad, H. Aruga Katori, and A. Ito, Phys. Rev. Lett. **74**, 4305 (1995).
[20] I. S. Suzuki and M. Suzuki, Phys. Rev. B **72**, 104429 (2005).
[21] C. Rigaux, Ann. Phys. (Paris) **20**, 445 (1995).
[22] I. S. Suzuki and M. Suzuki, Phys. Rev. B **68**, 094424 (2003).
[23] L. Lundgren, in *Relaxation in Complex Systems and Related Topics*, edited by L. A. Campbell and C. Giovannella (Plenum Press, New York, 1990), p. 3.
[24] J. A. Mydosh, *Spin Glasses—An Experimental Introduction* (Taylor and Francis, London, 1993).
[25] G. M. Wannier, Phys. Rev. **79**, 357 (1950).
[26] H. Kawamura and S. Miyashita, J. Phys. Soc. Jpn. **53**, 4138 (1984).
[27] I. S. Suzuki and M. Suzuki, Phys. Rev. B **59**, 6943 (1999).
[28] M. Campostrini, M. Hasenbusch, A. Pelissetto, P. Rossi, and E. Vicari, Phys. Rev. B **65**, 144520 (2002).
[29] M. F. Collins, *Magnetic Critical Scattering* (Oxford University Press, New York, 1989).
[30] Y. Yeshurun, M. B. Salamon, K. V. Rao, and H. S. Chen, Phys. Rev. B **24**, 1536 (1981).
[31] S. Pouget, M. Alba, and M. Nogues, J. Appl. Phys. **75**, 5826 (1994).
[32] A. B. Harris, J. Phys. C **7**, 1671 (1974).
[33] M. D. D. Meo, J. D. Reger, and K. Binder, Physica A **220**, 628 (1995).
[34] A. G. Berndt, X. Chen, H. P. Kunkel, and G. Williams, Phys. Rev. B **52**, 10160 (1995).
[35] A. G. Berndt, H. P. Kunkel, and G. Williams, J. Phys.: Condens. Matter **10**, 8535 (1998).